Multiphysics Simulation of Conjugated Heat Transfer and Electric Field on Application of Electrostatic Chucks (ESCs) Using 3D-2D Model Coupling

Kuo-Chan Hsu[1], Chih-Hung Li[1], Jaw-Yen Yang[1,2*], Jian-Zhang Chen[1], Jeng-Shian Chang[1]

[1]Institute of Applied Mechanics, National Taiwan University, Taiwan
[2]Center for Advanced Study in Theoretical Sciences, National Taiwan University, Taiwan
[*]Corresponding author: No.1, Sec.4, Roosevelt Road, Taipei 106, Taiwan, jawyen.yang@gmail.com

ABSTRACT: In recent years, there has been considerable interest in the electrostatic chucks (ESCs). Wafer cooling by means of gas at the backside of wafers plays an important role in electrostatic chucks and it uses an electrostatic potential to secure the wafer. In this study, the correlation of the electric voltage and electrostatic force distribution are considered to the ability of heat conductance. For this purpose, multiphysics simulation has been carried out to study the influence of electrostatic on temperature distribution of a wafer. The resulting temperature distribution on a wafer held by a ceramic body of the electrostatic chuck is investigated and conduct the conjugated heat transfer in 3D and electrostatic force is presented in 2D.

Keywords: Multiphysics, Conjugated heat transfer, Electric field, Electrostatic chucks (ESCs), Temperature

1. INTRODUCTION

With science and technology improvement, lower and uniformity distribution of wafer temperature are required due to film growing and yield rate for semiconductor processing equipment [1][2]. For this purpose, electrostatic (so-called ESCs) is one of the solutions. The electrostatic chucks mainly constructed of a ceramic material with high thermal conductivity and embedded tungsten electrode within chucks. An electrostatic force is established by applying an electric potential to both of the electrodes. There are mainly two of the heat transfer path to remove the heat from the wafer: (a) Cooling gas (usually helium) is introduced through a hole on the bottom of chuck and force the part of heat out of the wafer. (b) Flowing cooling liquid on the specific geometry of channel, under ceramic chuck and bring the else of heat out of the ceramic body.

This paper presents both conjugated model (heat transfer and fluid dynamics) and electrostatic model. The model is developed to predict the wafer temperature distribution under various potential voltage of electrodes embedded within chucks. It is found that control of thermal resistances across the interface between the wafer and the surface of chuck plays an important role in controlling both of the top temperature and temperature uniformity. Also, build up a correlation between the wafer temperature and potential voltage, from the simulation results.

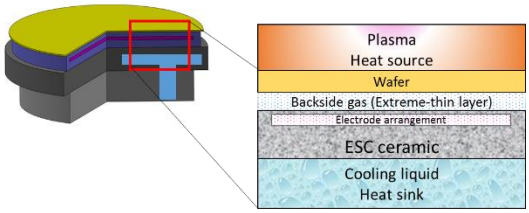

Figure 1. Schematic presentation of electrostatic chuck. An electrode arrangement is embedded within the ceramic body and the wafer has an intimated contact to the chuck with electrostatic attractive force.

2. GOVERNING EQUATIONS

The analysis of the model utilizes the built-in conjugated model and electrostatic model available in COMSOL Multiphysics. The derivations of these equations have been well documented in literature. However, they are presented here for completeness.

2.1 Heat transfer path in both groove region and contact region.

When both of the objects are pressed together, no two solid surface will ever form a perfectly contact region due to machining limitations. The aim of the section is to predict h_{sum} that dependent upon the characteristics of the surface, the mechanical pressure between them, and whether there is any conducting fluid in the interstices of the interface [3][4]. The CMY model was extend to include the effect of high thermal conductivity layers and contact micro hardness was depend on material properties, surface roughness parameters, and contact pressure. It considers the resistance to the flow of heat between two solid bodies in contact and

reported that the available simple contact conductance model was expressed as [5][6]:

$$h_{sum} = h_{solid} + h_{fluid} \quad (1)$$

Where h_{sum}, h_{solid} and h_{fluid} are the joint, solid and fluid conductance, respectively. This simple relation shows that there are two paths for the heat to cross the joint: (i) by the means of the micro contacts and (ii) gas across the micro gaps. Radiation heat transfer across the micro and macro gaps was ignored.

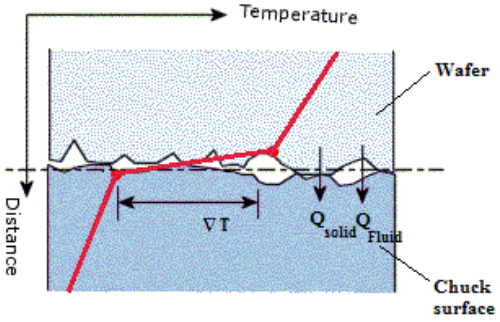

Figure 2. Temperature drop through the interface between the two contacting faces and two modes of heat transfer exist. The first is conduction through points of solid-to-solid contact (Q_s). Secondly, conduction through the gas filled gaps (Q_c).

2.2 Navier-Stokes (N-S) equations

In differential form, the N-S equations are given by:

$$\rho \frac{D\mathbf{u}_f}{Dt} = -\nabla p + \mu \nabla^2 \mathbf{u}_f + \mathbf{F}_f \quad (2)$$

and

$$\nabla \cdot \mathbf{u}_f = 0 \quad (3)$$

where Eq. (1) represents the conservation of momentum and Eq. (2) represents the conservation of mass. The subscript, *f*, denotes the fluid domain. The majority of the flows simulated for the problems considered here are laminar flow. The boundary conditions imposed on the momentum balance are no slip at the walls:

$$P = P_0 \qquad \text{Inlet}$$

$$u = 0 \qquad \text{Walls}$$

No slip boundary condition for a stationary solid wall means the fluid at the wall is not moving. The outlet boundary conditions describing fluid flow at an outlet are the pressure, and no viscous stress. The pressure condition prescribes only a Dirichlet condition for the pressure:

$$P = 1\ atm \qquad \text{Outlet}$$

The boundary conditions are physically equivalent to a boundary that is adjacent to a large container (inlets) or existing into a large container (outlets).

2.3 Maxwell stress tensor equations

Wafer is secured on the top of electrostatic chuck by applying potential voltage of the electrodes and the electrostatic force can be introduced from Maxwell stress tensor. The total electromagnetic force on the charges in volume *V* is:

$$F = \int_V (E \times v \times B)\rho d\tau = \int_V (\rho E + J \times B) d\tau \quad (4)$$

This equation could be simplified by introducing the Maxwell stress tensor T. The Maxwell stress tensor is a second rank tensor used in classical electromagnetism to represent the interaction between electromagnetic forces and mechanical momentum[7]:

$$T_{ij} \equiv \epsilon_0 \left(E_i E_j - \frac{1}{2}\delta_{ij} E^2 \right) + \frac{1}{\mu_0}\left(B_i B_j - \frac{1}{2}\delta_{ij} B^2 \right) \quad (5)$$

The i and j are the coordinates of x,y and z, so the Maxwell stress tensor T are composed of nine components.

3. BOUNDARY CONDITIONS

The thermal process can be explained as follows: uniform heat source is applied to the wafer surface and piece of heat is brought out from the wafer by means of backside gas and flowing liquid. In this study, we are working on the following assumptions to simplify model: (i.) stationary state (ii.) thermal insulation in the chamber (iii.) neglect the heat radiation effect (iv.) uniform heat source from plasma to the wafer (v.) neglect the heat of chemical reaction on wafers. In addition, all of materials in this study are listed in table 1. Two of the ceramic materials are shown in column 1 and 2. Pedestal, an interface between wafer and electrostatic chuck, is made up with Al alloy. Neglect the thermal resistance resulted

from tungsten electrodes due to the extreme-thin thickness.

	AlN	Al_2O_3	Al6061	Si
Thermal Conductivity @20[$^W/_{mK}$]	180.0	35	167.0	150.0
Coefficient of thermal expansion[$^{10^{-6}}/_{°C}$]	6.8	8.1	23.0	5.0

Table 1. Thermal conductivity and thermal expansion coefficient of materials in this model.

3.1 Conjugated heat transfer

The principle of set-up is shown in Figure 3. The setting of simulation: pure water as the working fluid, the pressure drop of fluid maintains 30 torr and the inlet temperature is 288K. The fluid property is seen as laminar fluid since the Reynolds number is roughly derived as magnitude 230 from simulation results. Therefore, conditions of no viscous fluid and incompressible fluid are reasonable to be considered in this problem. The general inward heat flux is 1.414 W/cm^2, uniformly applied to the top of wafer. For backside cooling, the effect of heat transfer due to moving fluid is replaced as the heat convection on the groove surface and the magnitude of heat convection coefficient can be derived from [6]. The roughness of ESC surface of Al_2O_3 ceramic body is varied by a factor of 2, and it is much greater than that of AlN.

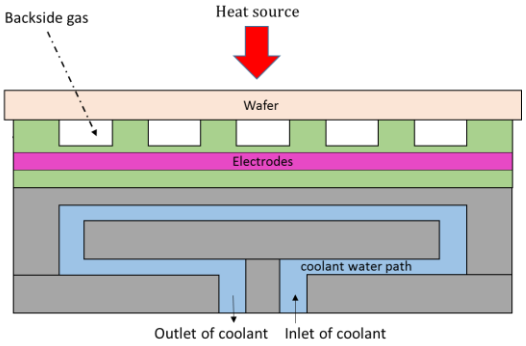

Figure 3. Rough schematic cross-sectional presentation of electrostatic chucks and some of the explanations of boundary conditions.

3.2 Electrostatic interface

The principle of set-up is shown in Figure 4. We divided it by following steps: (i) locate the boundary section of electrode A and B at constant potential voltage +/-2.0, +/-2.5 and +/-3.0 kV separately. (ii) make both top and bottom of entire model (geometry) connect to ground in order to balance the electron balance. (iii) for charge density, both sides of gap resulted from roughness are forced to zero (iv) periodic condition is applied to both sides of entire model (geometry) due to reduction of the element numbers. However, the edge effect on electric distribution field is ignored.

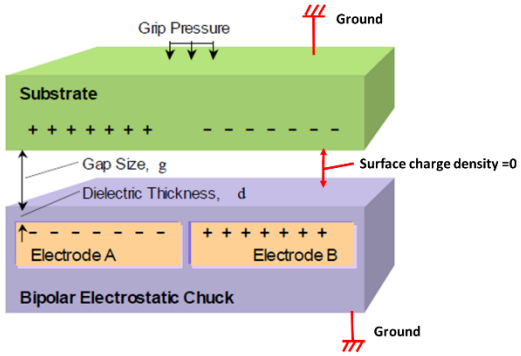

Figure 4. Schematic presentation of bipolar electrodes arrangement and boundary conditions.

4. RESULTS AND COMPARISON

Multiphysics simulation has been carried out to study the influence of electrostatic and helium backside pressure on temperature distribution of a wafer. This section is separated in three parts. First, we present the results of the wafer temperature distribution and the improvement compared with two ceramic bodies (AlN and Al_2O_3) in Figure 5 – 8. Secondly, the electrostatic force and electric field on the wafer in various potential voltage in Figure 9 – 10. Finally, we sketch a plot to analyze the temperature improvement due to the magnitude of backside helium pressure and electric potential in Figure 11 – 12.

4.1 Wafer temperature distribution

Both of the results reveal that the highest temperature occurs at the edge of wafer. Resulted from the radius of ESC should be slightly less than that from wafer in deposited processing applications so as to cover the ESC surface from metal deposition. In our study, the radius of ESC is about 2% smaller than wafer. Due to the wafer overhang, the wafer temperature is increasing desperately on edge since there are no backside cooling and contact regions, rarely thermal conduction surrounding edge regions.

From the results of Figure 5 and Figure 7, for ceramic body of AlN material, it is obvious that average wafer temperature is lower than Al_2O_3.

Besides, the lowest temperature of wafer (deep blue) occurs near the inlet cooling liquid and quickly cooling down (color change). The main reason is that natural high thermal conductivity of AlN ceramic is capable of removing the great part of heat energy out of the wafer that finally transferred to cooling water. In other words, the cooling liquid brought more heat energy out of the system and increase water temperature distinctly than ESC with Al_2O_3.

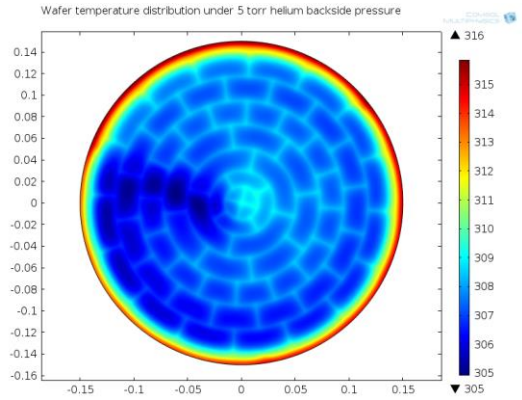

Figure 5. Wafer temperature distribution, ceramic body of AlN.

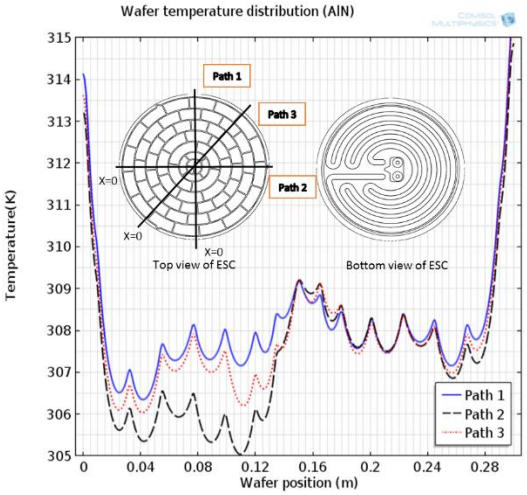

Figure 6. Wafer temperature distribution in three of the paths from edge (0 mm) to edge (300 mm) for AlN ceramic body. This pattern is used to create "contact regions" where the wafer and chuck form an intimate contact and "grooved regions" whose the depth is below 100μm.

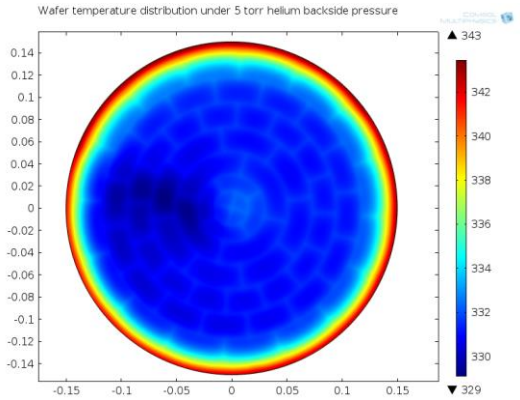

Figure 7. Wafer temperature distribution, ceramic body of Al_2O_3

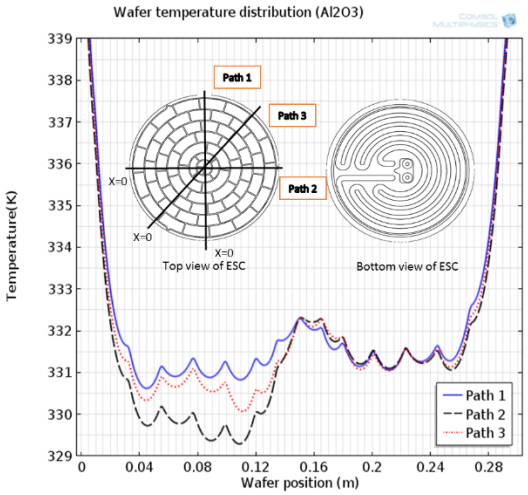

Figure 8. Wafer temperature distribution in three of the paths from edge (0 mm) to edge (300 mm) for Al_2O_3 ceramic body.

From the results of Figure 6 and Figure 8, we sketched three of the paths to reveal the temperature distribution within the wafer. The non-symmetrical temperature distribution mainly resulted from the geometrical design of cooling liquid (water). According to the comparison of the two ceramic bodies, the wafer temperature around the edge regions is relative higher than that around central regions especially for Al_2O_3 ceramic body.

4.2 Electrostatic force and electric field distribution

As shown in Eq. (5), the attractive force is always normal to the object. Therefore, the net electrostatic force upon the wafer should be the differences between the top and bottom wafer. From the result of simulation, we found the

electrostatic pressure and electric field will rapidly drop on both edges of electrodes. As shown in Figure 9, the electrostatic pressure right above the electrodes is approximately proportional to the square of potential voltage between the electrodes.

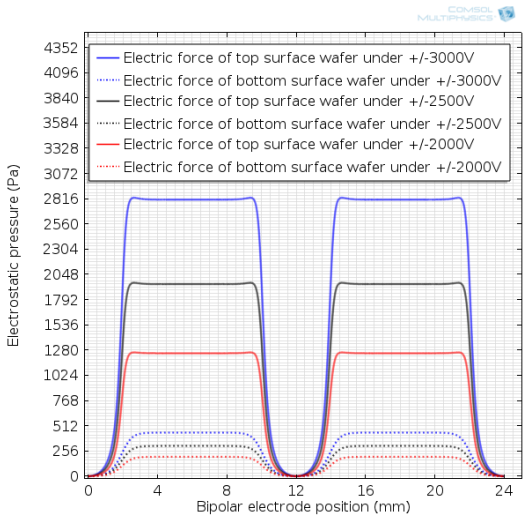

Figure 9. Electrostatic pressure versus the potential voltage.

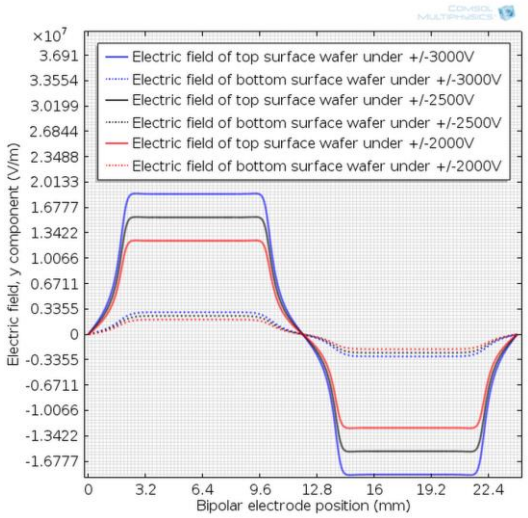

Figure 10. Electric field versus the potential voltage.

4.3 Correlation between wafer temperature uniformity, backside pressure and electric potential

Generally speaking, the force equilibrium is based on three factors: electrostatic force, wafer mass and backside pressure. Some points are missing at the end of line in Figure 11 as backside pressure raise. It means the force equilibrium is unsatisfied; consequently, electrostatic force is unable to secure the wafer remain stationary as the backside pressure increase due to the backside pressure becomes attractive force.

From Figure 11, we have divided the discussions into three parts: (i.) the improvement of wafer temperature non-uniformity will be better as the backside pressure increase. However, for ceramic body of AlN, it is indistinct to lessen the non-uniformity by controlling the backside pressure. The main reason is the principal heat energy transferred to cooling liquid (water) via ceramic body with higher thermal conductivity – AlN. (ii.) at specific backside pressure, the temperature non-uniformity lessens when potential voltage increases. From the relation between electrostatic force and voltage, the more electrostatic force secures the wafer, the more potential voltage applies to electrodes. With higher clamping force on the wafer, more area with solid conductivity will be available that is beneficial for heat transfer.

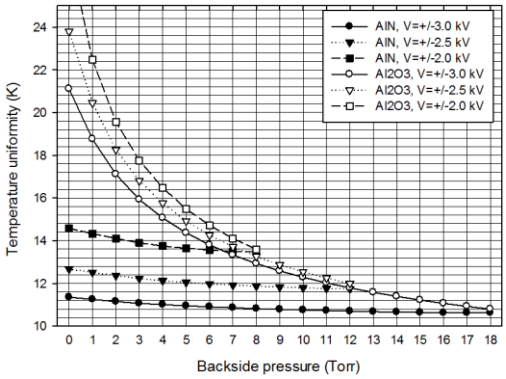

Figure 11. Wafer temperature uniformity versus the backside gas pressure in two ceramic materials when the electric potential range from 2.0 to 3.0 kV.

(iii.) at specific backside pressure, the top temperature slightly raises as backside pressure increases. Since the overpressure will induce the wafer to break away the chuck a little, less available area with solid conductivity is disadvantageous to heat transfer. Nevertheless, for ceramic body of Al_2O_3, the principal heat transfer to cooling down depends on the backside gas.

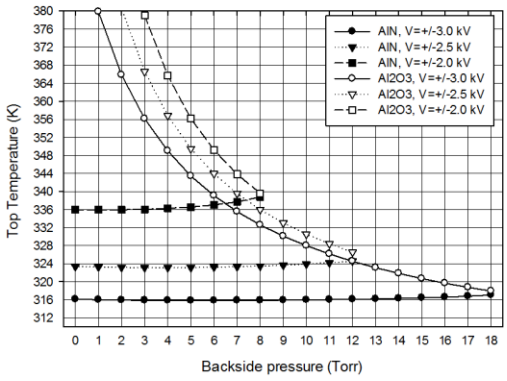

Figure 12. Top wafer temperature versus the backside gas pressure in two ceramic materials when the potential electric range from 2.0 to 3.0 kV.

4 CONCLUSIONS

As mentioned above, we summarize the results into five points: (i.) The AlN ceramic body significantly reduce the wafer temperature and non-uniformity other than Al_2O_3 one. (ii.) The non-symmetrical temperature distribution mainly results from the geometric design of cooling water. (iii.)The electrostatic voltage is a principal factor of wafer temperature and distribution. (iv.)The top temperature slightly increases as backside pressure due to the less available area of ESCs to the wafer. (v.)The relation of the electrostatic force and potential voltage is built up.

5 REFERENCES

[1] K. Yatsuzuka, F. Hatakeyama, K. Asano, S. Aonuma, Fundamental characteristics of electrostatic wafer chuck with insulating sealant, IEEE. Trans. Ind. Appl. 36 (2000) 510-516.

[2] K. A. Olson, D. E. Kotecki, A. J. Ricci, S. E. Lassig, A. Hussian, Characterization, modeling, and design of an electrostatic chuck with improved wafer temperature uniformity, Rev. Sci. Instrum. 66 (1995) 1108.

[3] M. M. Yovanovich, Four decades of research on thermal contact, gap, and joint resistance in microelectronics, IEEE Trans. Compon. Packag. Technol. 28 (2005) 182-206.

[4] V. W. Antonetti, M. M. Yovanovich, Using metallic coatings to enhance thermal contact conductance of electronic packages, Heat Transfer Eng. 9 (1983) 85-92.

[5] V. W. Antonetti, M. M. Yovanovich, Using metallic coatings to enhance thermal contact conductance of electronic packages, Heat Transfer Eng. 9 (1983) 85-92.

[6] M. Klick, M. Bernt, Microscopic approach to an equation for the heat flow between wafer and E-chuck, J. Vac. Sci. Technol. B 24 (2006) 2509-2517.

[7] Y. D. Lim, D. Y. Lee, W. J. Yoo, Temperature of a semiconducting substrate exposed to an inductively coupled plasma, J. Korean Phys. Soc. 59 (2011) 262-270.

6 ACKNOWLEDGEMENTS

The authors gratefully acknowledge the funding by National Chung-Shan Institute of Science & Technology (NCSIST) and the assistance of Leading Precision Inc. (LPI). We are also thankful to Institute of Applied Mechanics (IAM) for software offering.